THE JOURNAL OF BIOLOGICAL CHEMISTRY
Vol. 273, No. 32, Issue of August 7, pp. 20276–20284, 1998
Printed in U.S.A.


# Evidence for Dinucleotide Flipping by DNA Photolyase*

(Received for publication, March 9, 1998, and in revised form, May 25, 1998)

**Brian J. Vande Berg‡ and Gwendolyn B. Sancar§**

*From the Department of Biochemistry and Biophysics, University of North Carolina School of Medicine, Chapel Hill, North Carolina 27599-7260*

**DNA photolyases repair pyrimidine dimers via a reaction in which light energy drives electron donation from a catalytic chromophore, $FADH^-$, to the dimer. The crystal structure of *Escherichia coli* photolyase suggested that the pyrimidine dimer is flipped out of the DNA helix and into a cavity that leads from the surface of the enzyme to $FADH^-$. We have tested this model using the *Saccharomyces cerevisiae* Phr1 photolyase which is >50% identical to *E. coli* photolyase over the region comprising the DNA binding domain. By using the bacterial photolyase as a starting point, we modeled the region encompassing amino acids 383–530 of the yeast enzyme. The model retained the cavity leading to $FADH^-$ as well as the band of positive electrostatic potential which defines the DNA binding surface. We found that alanine substitution mutations at sites within the cavity reduced both substrate binding and discrimination, providing direct support for the dinucleotide flip model. The roles of three residues predicted to interact with DNA flanking the dimer were also tested. $Arg^{452}$ was found to be particularly critical to substrate binding, discrimination, and photolysis, suggesting a role in establishing or maintaining the dimer in the flipped state. A structural model for photolyase-dimer interaction is presented.**

Pyrimidine bases absorb strongly in the UV region and are highly susceptible to photochemical reactions that alter their structures. In DNA, cyclobutane pyrimidine dimers (CPDs)[1] and pyrimidine-pyrimidone (6-4) photoproducts are the most frequent and biologically significant products of these reactions. These lesions are lethal and mutagenic and must be repaired to ensure cell survival and genetic stability. DNA photolyases repair CPDs and (6-4) photoproducts via reactions in which near UV or visible light provides the energy for bond rearrangements which restore the pyrimidines to their undamaged state. Two types of DNA photolyases have been recognized with regard to substrate specificity as follows: cyclobutane dipyrimidine photolyases and (6-4) photolyases (see Ref. 1 for a recent review). Each type of enzyme recognizes and efficiently repairs a single type of damage (2, 3). The cyclobutane dipyrimidine photolyases, hereafter referred to as CPD photolyases, are the subject of this report.

Understanding how the CPD photolyases efficiently repair pyrimidine dimers in DNA entails answering the following two questions: how do the enzymes recognize pyrimidine dimers specifically in the midst of a vast excess of nondamaged bases, and how do the enzymes catalyze dimer photolysis? Photolysis involves two noncovalently bound chromophores, reduced FAD and a second chromophore which, depending upon the source of the enzyme, is either folate or deazaflavin (4). Absorbance of a photon of photoreactivating light subsequent to substrate binding initiates electron donation by enzyme-bound $FADH^-$ to one of the bases in the dimer (4, 5). The photon may be absorbed either directly by $FADH^-$ or, more often, by the second chromophore which transfers energy to the flavin chromophore (1). Both electron transfer and energy transfer are highly efficient processes, resulting in a quantum yield for the overall photolysis reaction of 0.6–1.0 for CPDs containing thymine or uracil (6, 7).[2]

CPD photolyases are structure-specific enzymes that display binding discrimination comparable to that seen for sequence-specific DNA-binding proteins. Studies on the *Escherichia coli* and *Saccharomyces cerevisiae* enzymes have shown that the equilibrium association constant for (*cis,syn*)-CPDs in DNA is approximately $10^9$ $M^{-1}$, whereas the association constant for nondamaged DNA is $10^3$ $M^{-1}$ (6, 8–10). The affinity for (*trans,-syn*)-pyrimidine dimers in DNA and U<>U dimers in RNA is only about 10-fold greater than that for nondamaged DNA; nevertheless, once bound, these lesions are photolyzed efficiently (7, 11). Thus the presence of a cyclobutane dimer, the geometry of the bases in the dimer, and the absence of a 2′-OH on the sugar phosphate backbone are determinants of binding specificity. Important recognition elements are also found in DNA flanking the dimer. In particular, ethylation of the first phosphate 5′ to the dimer and 3–4 phosphates 3′ to the dimer in the lesion-containing strand inhibits binding (12, 13). At least some of these interactions contribute to binding specificity as shown by the fact that discrimination between dimer-containing and undamaged oligonucleotides decreases as the substrate is shortened (6). In addition, mutations in the yeast Phr1 photolyase have been identified which simultaneously decrease substrate discrimination and alter interactions with DNA phosphates surrounding the dimer (9). These results imply that the structure of the flanking sugar-phosphate backbone is uniquely altered by the dimer.

A structural basis for the efficiency of the photolysis reaction and for specific substrate recognition has been provided by the crystal structure of *E. coli* photolyase (14). The polypeptide chain is folded into an amino-terminal $\alpha/\beta$ domain and a carboxyl-terminal helical domain with the folate cofactor nestled into a shallow cleft between the two domains. The flavin chromophore lies deeply buried in the center of the helical domain,

* This work was supported by Grant GM35123 from the National Institutes of Health. The costs of publication of this article were defrayed in part by the payment of page charges. This article must therefore be hereby marked "*advertisement*" in accordance with 18 U.S.C. Section 1734 solely to indicate this fact.

‡ Current address: Laboratory of Structural Biology, NIEHS, National Institutes of Health, P. O. Box 12233, MD F3–01, Research Triangle Park, NC 27709-2233.

§ To whom correspondence should be addressed. Tel.: 919-966-2077; Fax: 919-966-2852; E-mail: gsancar.biochem@mhs.unc.edu.

[1] The abbreviations used are: CPDs, cyclobutane pyrimidine dimers; FAD, flavin adenine dinucleotide; Phr1, photolyase encoded by the *S. cerevisiae PHR1* gene; EMSA, electrophoretic mobility shift assay; LPCR, polymerase chain reaction; bp, base pair(s).

[2] A. Sancar, personal communication.

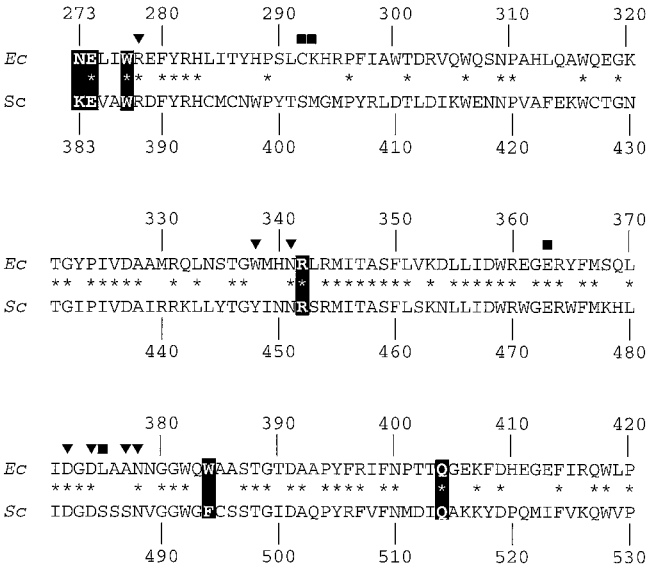


FIG. 1. **Alignment of *E. coli* and *S. cerevisiae* photolyases over the region modeled for the yeast Phr1 photolyase.** *Numbering above* and *below* the sequences refer to the positions in the *E. coli* and yeast enzymes, respectively. Identities are indicated by *. Sites of interaction (direct or water-mediated hydrogen bonds) between the apoenzyme and the flavin (▼) and folate (■) chromophores in the *E. coli* crystal structure are marked. Amino acids selected for alanine substitution mutagenesis (yeast amino acids $Lys^{383}$, $Glu^{384}$, $Trp^{387}$, $Arg^{452}$, $Phe^{494}$, and $Gln^{514}$) are shown enclosed in *black boxes*. $Lys^{330}$ was also modeled and mutated.

with direct access to solvent limited to a cavity leading from the edge of the isoalloxazine ring of flavin to the surface. The cavity lies in the center of a trace of positive electrostatic potential that runs along the flat face of the helical domain, and both the dimensions of the cavity and the asymmetric distribution of hydrophobic and polar residues within the cavity are appropriate to accommodate a pyrimidine dimer. These features of the photolyase structure led Park and co-workers (14) to propose that *E. coli* photolyase binds DNA along the trace of positive electrostatic potential and that in the enzyme-substrate complex the dimer is flipped out of the DNA helix and into the cavity leading to FAD. Here we report the results of mutational studies designed to test the model for photolyase binding using the yeast Phr1 photolyase. Phr1 and *E. coli* photolyases contain identical chromophores and are 50% identical in primary sequence over the region encompassing most of the proposed DNA binding surface and the cavity leading to flavin. Our results provide the most detailed picture yet of interactions at the photolyase-DNA interface, support the dinucleotide flip model, and suggest that interactions between DNA and residues inside and outside of the cavity contribute to binding affinity, to substrate discrimination, and to maintaining the dimer in the flipped state.

## EXPERIMENTAL PROCEDURES

*Protein Modeling*—Modeling was performed using the program FRODO (PSX, version 6.6) on an Evans and Sutherland PS300 Graphics system. The *E. coli* photolyase crystal structure (see Ref. 14; Protein Data Base code 1dnp) was used as the starting point for modeling the structure of the DNA-binding site of yeast photolyase. The region of the $\alpha$-helical domain of *E. coli* photolyase encompassing helices 11 through 18 (amino acids 273–419) contains most of the residues predicted to interact with DNA in and surrounding the cavity leading to the flavin chromophore (14). Within this region the overall sequence identity between the two enzymes is 50% (Fig. 1). To model this region, the 73 nonidentical amino acids in the *E. coli* photolyase sequence were replaced with the corresponding amino acids from the *S. cerevisiae* Phr1 sequence (15). Each new amino acid was subjected to a modeling and refinement protocol. First, the amide nitrogen, $\alpha$ carbon, and amide carbon of each amino acid were placed in the position of the previous *E. coli* amino acid. The yeast amino acid side chain was then rotated about its first dihedral rotation angle ($\chi_1$) to produce an alignment devoid of steric clash. Because $\chi_1$ displays a strong tendency to assume values near 60, 180, and 300°, each new side chain was examined first in each of these positions. The preferred alignment was at a $\chi_1$ value that placed the yeast side chain near the *E. coli* side chain and did not produce any steric clashes (within 2.5 Å). At positions 285, 291, and 368 (Phr1 positions 395, 401, and 478), alternative values for $\chi_1$ had to be chosen. A similar protocol was used to model the dihedral angle $\chi_2$ between the $\beta$ and $\gamma$ carbons on Gln, Glu, Lys, Arg, Met, Phe, Tyr, and Trp side chains. Again, the preferred dihedral values were those that placed the yeast side chain near the corresponding *E. coli* side chain. Steric clashes at positions 307, 308, and 411 (Phr1 positions 417, 418, and 521) prohibited placing these side chains in the preferred positions. The program REFINE, written by Dr. Jan Hermans (University of North Carolina, Chapel Hill), was then used to refine the geometry (bond lengths, bond angles, and dihedral angles) for the *S. cerevisiae* model. Individual amino acids were first refined, then the entire structure was analyzed over the course of 10 cycles. After 10 cycles, the cumulative coordinate shift was determined, and further modeling was performed until this shift value decreased to less than 5.0 Å. An identical approach was used to replace $Arg^{226}$, which lies near the rim of the cavity leading to flavin, with the equivalent yeast residue, $Lys^{330}$.

*Construction of PHR1 Mutants*—The entire *PHR1* coding region and approximately 500 bp of 3′-flanking sequence were subcloned from pCB1241/recon (9) into *Xmn*I-*Pst*I-digested pMal-c2 (New England Biolabs), yielding pGBS424. Oligonucleotides used in the construction of the various mutants are listed in Table I, and the locations of the introduced mutations and relevant restriction sites are shown in Fig. 2. To facilitate construction of the K330A mutant, PCR mutagenesis was used to introduce a *Sma*I site into *PHR1* at nucleotides 684–689 (relative to the first *PHR1* ATG; Fig. 2), yielding plasmid pGBS425. The amino acid sequence of photolyase was not changed in this construction. Alanine substitution mutations were introduced at $Lys^{330}$, $Glu^{384}$, $Arg^{452}$, $Phe^{494}$, and $Gln^{514}$ using two-primer ($Lys^{330}$, $Arg^{452}$) or four-primer PCR mutagenesis ($Lys^{383}$, $Glu^{384}$, $Phe^{494}$, and $Gln^{514}$) and pGBS425 as template. Vent DNA polymerase (New England Biolabs) was used in the first PCR stage (25 cycles). For 4-primer PCR, the first stage PCR products were purified on 3% GTG agarose gels (FMC Bioproducts), recovered in sterile water, and used for the second PCR reaction in conjunction with appropriate outside primer pairs (Table I). Amplification was carried out for 15 cycles using *Taq* polymerase (Life Technologies, Inc.). Purified PCR products were digested with appropriate restriction endonucleases and cloned into pGBS425 which had been digested with the same set of enzymes as follows: *Kpn*I and *Xba*I for K383A and E384A, *Xba*I and *Pst*I for F494A and Q514A, *Kpn*I and *Xba*I for R452A, and *Sma*I and *Kpn*I for K330A (Fig. 2). In each case the nucleotide sequence of the amplified region was verified to ensure that no additional mutations were introduced by the PCR. The photolyase bearing three substitutions (K330A/E384A/F494A) was constructed by subcloning restriction fragments containing the E384A and the F494A mutations into the K330A plasmid using unique restriction sites surrounding each mutation. To express *PHR1* without any attached fusion protein, the ~2.4-kilobase pair *Bgl*II-*Pst*I fragment from each mutant was subcloned into similarly digested pCB1241/recon. Construction of mutant W387A has been described previously (9).

*Photolyase Purification and Spectral Characterization*—All photolyases were overexpressed from pCB1241/recon derivatives (no maltose binding protein fusion) in *E. coli* strain CSR603F′$lacI^{Q}$ ($Phr^{-}$) and purified as described previously to greater than 95% purity as judged by Coomassie Blue staining (9). The protein concentration and chromophore content for each protein preparation were determined by spectroscopy from 220 to 700 nm (9). The spectra were closely examined for the presence of peaks near 450, 480, 580, and 625 nm, which are indicative of oxidation of the reduced flavin chromophore to the blue neutral radical or $FAD_{ox}$ (16).

*Quantitation of Specific and Nonspecific Equilibrium Association Constants ($K_A$, $K_S$, $K_{NS}$)*—A 43-bp DNA substrate containing a centrally located thymine dimer was prepared for these studies as shown in Oligonucleotide 1.

```
5′-pCTATCGATGGCCTGCAGGCAAGT<>TGGAGGAATTCGTACTGAGTC-3′
3′-  ATAGCTACCGGACGTCCGTTCA    ACCTCCTTAAGCATGACTCAGT-5′
```

OLIGONUCLEOTIDE 1

A (*cis,syn*)-thymidine dimer (a gift from Xiaodong Zhao and Aziz San-

TABLE I
*Oligonucleotides used for PCR mutagenesis of PHR1*

| Mutation introduced | Sequence[a] | Location[b] |
|---|---|---|
| *Sma*I site | Inside PCR primers | |
| | 5′-GTTGCTCCCGGGTTGATCACTACTG-3′ | 680–704 |
| | 5′-GTGATCAACCCGGGAGCAACAATGC-3′ | 699′–675′ |
| | Outside PCR primers | |
| | 5′-GCAGACTAATTCGAGCTCGAAC-3′ | pMAL |
| | 5′-CACTTAGCCCAGAGGTACCACCC-3′ | 1031′–1009′ |
| K330A | 5′-GTTGCTCCCGGGTTGATCACTACTG-3′ | 678–702 |
| | 5′-CAGAGGTACCACCCAAATATAGCATGTC***TGC***TTCATTG-3′ | 1018′–981′ |
| K383A | Inside PCR primers | |
| | 5′-CAAAATTTCATC***GCA***GAAGTTGCATG-3′ | 1135–1160 |
| | 5′-CAACTTC***TGC***GATGAAATTTTGGGTG-3′ | 1156′–1131′ |
| | Outside PCR primers | |
| | 5′-CTATATTTGGGTGGTACCTCTG-3′ | 997–1018 |
| | 5′-AGCTGTGATCATTCTAGATCTG-3′ | 1374′–1353′ |
| E384A | Inside PCR primers | |
| | 5′-CAAAATTTCATCAAA***GCA***GTTGCATG-3′ | 1135–1160 |
| | 5′-CAAC***TGC***TTTGATGAAATTTTGGGTG-3′ | 1156′–1131′ |
| | Outside PCR primers | |
| | 5′-CTATATTTGGGTGGTACCTCTG-3′ | 997–1018 |
| | 5′-AGCTGTGATCATTCTAGACCTG-3′ | 1374′–1353′ |
| R452A | 5′-CTATATTTGGGTGGTACCTCTG-3′ | 997–1018 |
| | 5′-CTGTGATCATTCTAGA***TGC***GTTATTAATATAG-3′ | 1372′–1341′ |
| F494A | Inside PCR primers | |
| | 5′-GTTGGTGGCTGGGGT***GCA***TGTTCTAGTACAG-3′ | 1465–1495 |
| | 5′-GTACTAGAACA***TGC***ACCCCAGCCACCAACATTTG-3′ | 1493′–1460′ |
| | Outside PCR primers | |
| | 5′-CTATATTAATAACAGGTCTAGAATGATCACAG-3′ | 1341–1372 |
| | 5′-GGCAGTGCCAAGCTTGCCTGCAG-3′ | 3′ to *PHR1* |
| Q514A | Inside PCR primers | |
| | 5′-GTTTTTAATATGGATATA***GCA***GCAAAAAAATATGAC-3′ | 1522–1557 |
| | 5′-CATATTTTTTTGC***TGC***TATATCCATATTAAAAACTC-3′ | 1555′–1520′ |
| | Outside PCR primers | |
| | 5′-CTATATTAATAACAGGTCTAGAATGATCACAG-3′ | 1341–1372 |
| | 5′-GGCAGTGCCAAGCTTGCCTGCAG-3′ | 3′ to *PHR1* |

[a] Underlined sequences denote restriction sites used in subsequent cloning steps. Sequences in bold italics denote mutations introduced into *PHR1*.

[b] With the exception of pMAL, sequence numbers correspond to those found in the *S. cerevisiae* genome database for the *PHR1* open reading frame. Numbers indicated with a prime symbol correspond to bottom strand (coding) sequences.

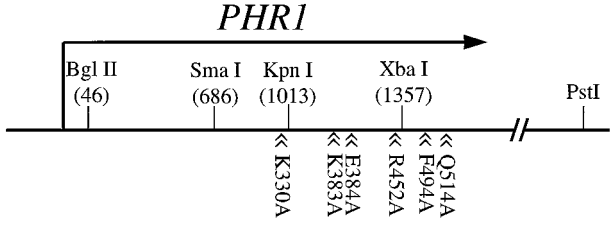


FIG. 2. **Map of the restriction sites used in constructing the *PHR1* mutations.** The direction of transcription of *PHR1* is indicated by the *arrow*. Restriction sites and their locations relative to the first base in the *PHR1* open reading frame are shown *above* the *line*, and the sites of PCR-generated mutations are shown *below* the *line*.

car) was synthesized and incorporated into the top strand oligonucleotide shown using standard oligonucleotide coupling protocols (17). Full-length oligonucleotide was purified from a denaturing polyacrylamide gel, quantitated by absorbance at 254 nm, and labeled at the 5′ end using T4 polynucleotide kinase and [$\gamma$-$^{32}$P]ATP (>6,000 Ci/mmol). The bottom strand oligonucleotide was quantitated by absorbance at 254 nm, and the two oligonucleotides were mixed at a concentration of 500 nM dimer oligonucleotide and 1500 nM bottom strand oligonucleotide in 20 mM Tris-HCl (pH 8.4), 50 mM KCl, heated at 90 °C for 5 min, and then allowed to anneal by slow cooling to room temperature. This procedure resulted in incorporation of >90% of the dimer oligonucleotide into double-stranded DNA. Oligo(dT)$_{18}$ (Sigma) dissolved in 10 mM Tris (pH 8.0), 1 mM EDTA was used as competitor for nonspecific binding studies.

For each photolyase preparation the fraction of photolyase molecules active in DNA binding was determined by titrating a fixed concentration of enzyme (2–3 × $K_D$) with increasing amounts of substrate, as described previously (9). Electrophoretic mobility shift assays (EMSAs) were used to separate bound and free substrate. Radioactivity present in the bound and free DNA bands was quantitated using an Ambis Radioanalytic Imager (Ambis Systems). The equilibrium association constants ($K_A$) of the various photolyases for the dimer-containing substrate were determined by titrating substrate ($5 \times 10^{-9}$ M) with enzyme (9). Control reactions without enzyme were used to calculate the amount of background smearing of the DNA in each gel. The slope of a Eadie-Scatchard plot (ES/$S_t$ × $E_f$ *versus* ES/$S_t$) of these data yielded $-K_A$ (where ES = bound DNA concentration; $S_t$ = total substrate concentration; and $E_f$ = free enzyme concentration). The binding affinity for nonspecific DNA ($K_{NS}$) was measured by titrating the enzyme-dimer oligonucleotide complex (70% of substrate bound in the absence of competitor) with cold oligo(dT)$_{18}$ over the nucleotide concentration range of $1 \times 10^{-4}$ M to $5 \times 10^{-3}$ M. The *x* intercept of a plot of 1/ES *versus* concentration of oligo(dT)$_{18}$ yielded $-(1/K_{NS})$ (18). $K_S$, the intrinsic specific association constant of photolyase for the dimer, was determined from the relationship $K_{obs} = K_S(1 + [D]K_{NS})$ where $D$= molar concentration of nondimer nucleotides in the 43-bp substrate (9). Each $K_A$, $K_{NS}$, and active molecule determination was performed at least 3 times.

*Ethylnitrosourea Interference*—End-labeled double-stranded dimer-containing substrate was ethylated at phosphate groups (19) as follows. 100 $\mu$l of ethanol saturated with ethylnitrosourea (Sigma) were added to 4 pmol of labeled substrate dissolved in 100 $\mu$l of sodium cacodylate (pH 8.0). Following incubation at 50 °C for 1 h, ethylnitrosourea was removed by seven ethanol precipitations in 0.5 M $CH_3CO_2NH_4$ with 25 $\mu$g of carrier RNA. The DNA was washed with 95% ethanol after the final precipitation, dissolved in 0.1 mM EDTA, and recovered substrate was quantitated by scintillation counting.

Electrophoretic mobility shift assays, in a volume of 100 $\mu$l, were performed using the conditions described above. $5 \times 10^{-9}$ M substrate was incubated with sufficient photolyase to produce 60% binding as judged by EMSA. Following EMSA, the bound and free DNAs were cut out of the gel, and the DNA was eluted by overnight agitation in 0.5 M $CH_3CO_2NH_4$, 1.0% SDS, filtered through glass wool, extracted with phenol and ether, and precipitated in ethanol. Following a second

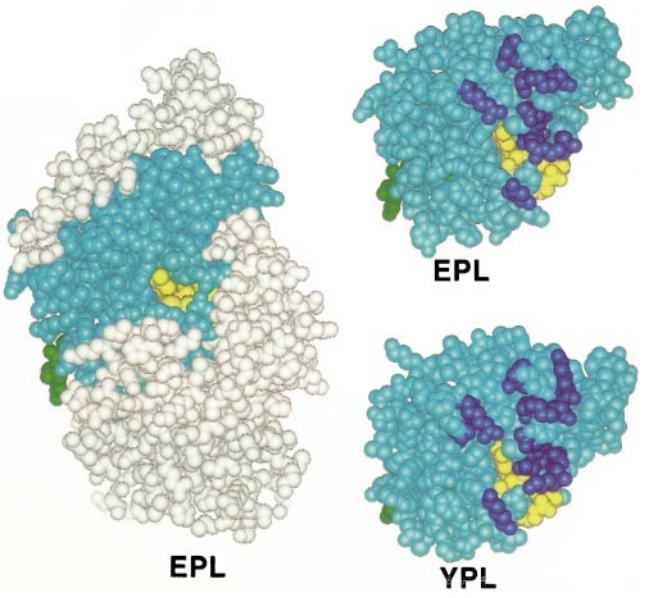


FIG. 3. **Structures of the DNA binding domains of *E. coli* and yeast photolyase.** Shown on the *left* is a space-filling model of *E. coli* photolyase (*EPL*) derived from the crystal structure. The view looks into the cavity that leads from the surface to $FADH^-$, which is shown in *yellow*. The folate chromophore, which is mostly hidden behind the protein, is shown in *green*. The region of EPL that was used to model the structure of the yeast photolyase (*YPL*) DNA binding domain is shown in *cyan*. On the *right*, the EPL pattern and the modeled YPL structure are enlarged to show the high degree of similarity between the structures. The band of positively charged amino acids that extend lengthwise across the faces of the structures is shown in *dark blue*.

ethanol precipitation and ethanol wash, the samples were lyophilized to dryness and then suspended in 15 $\mu$l of 10 mM $NaPO_4$ (pH 7.0), 1 mM EDTA. The DNA was cleaved at ethylated phosphates by addition of 2.5 $\mu$l of 1 M NaOH followed by incubation at 90 °C for 30 min. Fifteen $\mu$l of urea dye (6 M urea, 0.25% bromphenol blue) were added, and aliquots were loaded onto a 12% denaturing acrylamide gel alongside sequence ladders (A + G) (20). Band intensity was quantitated using a Molecular Dynamics PhosphorImaging System. To account for differences in loading, counts were normalized using as reference a band outside of the photolyase-binding site. The ethylnitrosourea interference pattern for each photolyase was determined twice.

*In Vitro Repair Assay*—Labeled 43-bp dimer-containing substrate was incubated in a volume of 300 $\mu$l with a sufficient concentration of wild-type or substituted photolyase to produce greater than 70% binding as measured by EMSA. Following a 20-min incubation in the absence of photoreactivating light, the binding reactions were placed in individual compartments in a 12-well microtiter plate and irradiated with 365 nm light (General Electric BLB) at a fluence rate of 2 $J/m^2/s$ (UV Products UV Radiometer with a 365-nm detector). Following each 25 J dose, a 25-$\mu$l aliquot was removed and loaded onto an EMSA gel. The amount of repair (increase in free substrate) following each dose was quantitated taking into account the amount of free substrate present prior to photoreactivation. The quantum yield for each photolyase was calculated as described previously (5, 9). Because the light source was not monochromatic, we have expressed the quantum yield for each enzyme relative to the quantum yield for the wild-type enzyme, rather than as an absolute value. A minimum of two experiments were performed for each photolyase.

## RESULTS

*Protein Modeling*—By using the crystal structure of *E. coli* photolyase (14) as a starting point, we modeled the structure of yeast Phr1 photolyase over the region encompassing residues 383 through 532 (*E. coli* photolyase residues 273–422; Figs. 1 and 3). The validity of this approach is supported both by the high degree of sequence conservation in these regions of the enzymes (50% identity with no gaps; Fig. 1 and see Ref. 15), which suggests a similar fold, and by the results obtained during the modeling. Of the 73 nonidentical residues replaced during modeling, only 6 residues (Phr1 residues 395, 401, 417, 418, 478, and 521) produced steric clashes when modeled using the torsion angles of the equivalent *E. coli* residue. Each of these residues could, however, be modeled using alternative standard torsion angles. Most of these residues are solvent-exposed and none lie near the proposed DNA binding surface or the flavin-binding site; therefore it is unlikely that an incorrect choice of torsion angle for these residues would affect either the overall accuracy of the model or the structure of either the DNA-binding site or the flavin-binding site. Overall the structures of the enzymes over the modeled region are highly similar to one another (Fig. 3), as well as to the recently solved *Aspergillus nidulans* photolyase structure (21). The latter enzyme exhibits 70% sequence identity to the *E. coli* photolyase within the modeled region (21).

Two important results relevant to this study emerged from the modeling of the yeast enzyme. (i) The structure of the flavin-binding site is conserved. Within the modeled region there are 6 amino acids that interact with FAD (14), 5 of which are identical to those found in the *E. coli* enzyme (Fig. 1). The single amino acid substitution ($Trp^{338}$(*E. coli*) → $Tyr^{448}$(*S. cerevisiae*)) places the $Tyr^{448}$ side chain OH within H-bonding distance of the same FAD phosphate contacted by the ring nitrogen of $Trp^{338}$ (data not shown). Of the seven FAD-contacting residues that lie outside of the modeled region (14), 5 are identical in both enzymes and one of the nonidentical amino acids ($Arg^{236}$(*E. coli*) → $Gly^{340}$(*S. cerevisiae*)) is predicted to make contact only through backbone substituents. The same substitution occurs in the *A. nidulans* photolyase structure where the FAD contact is conserved (21). Based upon the conservation of the cofactor-binding site, we conclude that the orientation of $FADH^-$ is likewise retained. (ii) The crucial features of the proposed DNA binding surface of the *E. coli* enzyme (14) are conserved in yeast photolyase (Fig. 3). This conservation is seen most strongly for residues lining the cavity leading from the surface to the flavin chromophore. The three substitutions, $Lys^{383}$(*S. cerevisiae*) → $Asn^{273}$(*E. coli*), $Phe^{494}$(*S. cerevisiae*) → $Trp^{384}$(*E. coli*), and $Lys^{330}$(*S. cerevisiae*) → $Arg^{226}$(*E. coli*), conserve the asymmetric distribution of polar and hydrophobic residues in the cavity. The band of positive electrostatic potential extending out from the cavity is also conserved and is augmented by several substitutions: $Lys^{383}$(*S. cerevisiae*) → $Asn^{273}$(*E. coli*), $Lys^{516}$(*S. cerevisiae*) → $Glu^{406}$(*E. coli*), and $Gln^{503}$(*S. cerevisiae*) → $Ala^{393}$(*E. coli*). The structural similarity of the proposed DNA binding surfaces of the yeast and *E. coli* enzymes is consistent with the fact that the footprints made by the enzymes on dimer-containing DNA are essentially identical (12).

Based upon the results of the modeling study, we selected $Phe^{494}$, $Glu^{384}$, $Lys^{330}$, $Lys^{383}$, $Arg^{452}$, and $Gln^{514}$ of *PHR1* as targets for alanine substitution mutagenesis. The first three residues lie within the active site cavity and are predicted to interact with a pyrimidine dimer flipped into the cavity, but they do not appear to interact directly with FAD. This latter observation is crucial to the interpretation of DNA binding data because mutations that destabilize flavin binding usually lead to unfolding of the enzyme.[2] $Lys^{383}$, $Arg^{452}$, and $Gln^{514}$ lie outside of the cavity and along the region of positive electrostatic potential on the proposed DNA binding surface (14). Based upon preliminary docking experiments (data not shown), these residues are likely to interact with the DNA flanking the dimer.

*Effects of Ala Substitutions on Substrate Binding and Discrimination*—Wild-type and alanine-substituted photolyases described above were purified and characterized by UV spectroscopy. Photolyase from the previously reported mutant

TABLE II
*Equilibrium binding constants for photolyase-DNA interaction and relative quantum yields for the photolysis reaction*

| Photolyase | Location of altered amino acid(s) | $K_A$[a] | $K_{NS}$[b] | Discrimination ratio[c] | Relative quantum yield at 365 nm[d] |
|---|---|---|---|---|---|
| | | $\times 10^8$ M$^{-1}$ | $\times 10^3$ M$^{-1}$ | $\times 10^5$ | |
| Wild-type | | 11.4 (±0.4) | 1.8 | 6.3 | 1.0 |
| K330A | Inside cavity | 6.3 (±1.0) | 0.9 | 7.2 | 1.1 |
| E384A | Inside cavity | 6.7 (±1.3) | 1.6 | 4.1 | 0.4 |
| F494A | Inside cavity | 4.5 (±1.4) | 1.3 | 3.5 | 0.7 |
| K330A/E384A/F494A | Inside cavity | 0.8 (±0.1) | 0.8 | 1.0 | 0.2 |
| W387A | Inside cavity | 0.7 (±0.1) | 0.6 | 1.1 | 0.2 |
| K383A | Outside cavity | 1.7 (±0.2) | 1.0 | 1.8 | 1.0 |
| R452A | Outside cavity | 0.6 (±0.1) | 3.1 | 0.2 | 0.4 |
| Q514A | Outside cavity | 0.4 (±0.1) | 0.7 | 0.6 | 0.9 |

[a] Affinity for a 43-bp substrate containing a single pyrimidine dimer. Standard errors are indicated in parentheses.
[b] Affinity per mol of nucleotide in oligo(dT)$_{18}$.
[c] Discrimination ratio = $K_S/K_{NS}$. Under our experimental conditions, $K_S = K_A/(1 + \sim 0.005)$, therefore $K_A$ was equated with $K_S$ for this calculation.
[d] Relative to the quantum yield of the wild-type enzyme.

W387A (9) was also purified and used for comparative purposes in all of the studies described below. For all enzyme preparations, both the folate and flavin chromophores were present in approximately equimolar (0.9–1.0) stoichiometry with the apoenzyme, and neither the flavin blue neutral radical nor oxidized flavin were detected (data not shown). Thus the overall structure of the enzyme was not perturbed in the mutants, the flavin-binding site was intact, and the normal oxidation state of the flavin chromophore was retained. The integrity of the flavin-binding site and retention of the normal oxidation state of the flavin chromophore are particularly noteworthy. The dinucleotide flip model predicts that the dimer interacts with both the adenine and isoalloxazine rings of flavin (14), and photolyase lacking flavin does not bind pyrimidine dimers with measurable affinity (22). Furthermore, although the redox state of flavin does not alter DNA binding, oxidation of the flavin chromophore to the blue neutral radical reduces the quantum yield of photolysis by an order of magnitude and enzyme containing oxidized FAD is inactive in photolysis (5, 22).

The equilibrium binding affinities of the photolyases for the 43-base pair substrate containing a single pyrimidine dimer were determined by EMSA. Each of the substituted photolyases displayed reduced affinity for the dimer (Table II). The $K_A$ values for enzymes bearing single substitutions in the active site cavity varied widely. Substitution at Lys$^{330}$, Phe$^{494}$, or Glu$^{384}$ produced a 40–60% decrease in affinity, whereas substitution of Trp$^{387}$ decreased binding 16-fold. These results suggest that individually Lys$^{330}$, Phe$^{494}$, and Glu$^{384}$ contribute little to the overall binding energy, whereas Trp$^{277}$ makes a major contribution. That these residues do indeed participate in binding was evident from the $K_A$ of the photolyase in which all three amino acids were substituted simultaneously with alanine. The reduction in binding affinity exhibited by the triple mutant (K330A/F494A/E384A) was comparable to that seen with the W387A mutant. Phe$^{494}$ and Glu$^{384}$ in particular are deeply recessed into the cavity and cannot contact any residue in normal B-DNA. In addition, both *E. coli* and yeast photolyase bind pyrimidine dimers in single-stranded DNA with an affinity similar to that seen with double-stranded DNA (6), which rules out binding to an extrahelical base in the complementary strand as a binding determinant. Therefore the reduced binding affinity exhibited by these mutants strongly supports the dinucleotide flip model for photolyase binding.

Substitutions outside of the active site cavity produced larger decreases in affinity (Table II). The $K_A$ for interaction between dimer-containing DNA and the K383A mutant was decreased approximately 7-fold, whereas $K_A$ values for R452A and Q514A decreased 21- and 29-fold, respectively. The large decrease in binding affinity seen with these mutants, compared with the smaller decreases seen with most of the cavity mutants, argues that much of the free energy of binding comes from interactions between photolyase and DNA flanking the dimer rather than from direct interaction with the dimer. This is consistent with previous observations suggesting that photolyase recognizes not only the dimer but also DNA structural components flanking the dimer (9, 12, 13).

The ability of a DNA-binding protein to recognize its specific target among an excess of nonspecific binding sites is determined by the ratio of the binding constants $K_S/K_{NS}$ (specific binding/nonspecific binding) known as the discrimination ratio. Among the photolyases bearing single substitutions in the cavity, only the W387A mutant displayed a large reduction in discrimination ratio (Table II). Once again synergy was observed with the triple mutant more severely compromised in substrate discrimination than any of the single cavity mutants including the W387A mutant. Two of the single substitutions outside of the cavity produced larger decreases in discrimination ratio than did any of the substitutions (single or multiple) inside the cavity (Table II). Particularly noteworthy is the R452A substitution which produced a 1.7-fold increase in $K_{NS}$ and 20-fold reduction in $K_S$. Among the 10 Phr1 substitution mutants now characterized (Ref. 9 and this work), this is the only mutant that exhibits an increase in $K_{NS}$. Clearly Arg$^{452}$ is a major determinant of binding specificity.

*Ethylation Interference Studies*—Interactions between photolyase and DNA phosphates surrounding the dimer contribute to both specific and nonspecific substrate binding (9). Ethylation of DNA phosphates interferes with these interactions either by eliminating a negative charge or by steric interference and is therefore a useful method for probing interactions at the binding interface. The results of ethylation interference studies on the mutant photolyases and wild-type enzyme are shown in Figs. 4 and 5. In previous studies we demonstrated that ethylation of the first phosphate 5′ to the dimer and the first through the fourth phosphates 3′ to the dimer interferes with binding by wild-type photolyase, whereas ethylation of the intradimer phosphate has no effect (9, 12). Interference at the fourth phosphate 3′ to the dimer is generally weak, and in the experiments reported here was not clearly discernible. In all other respects the ethylation interference pattern shown for wild-type photolyase in Fig. 4 is identical to those reported previously. In contrast, each of the mutants displayed changes in the ethylation interference pattern consistent with alterations in the binding interface.

Among the active site cavity mutants, two distinct patterns of altered ethylation interference were apparent (Fig. 5). Photolyases W387A and K330A exhibited decreased interference at

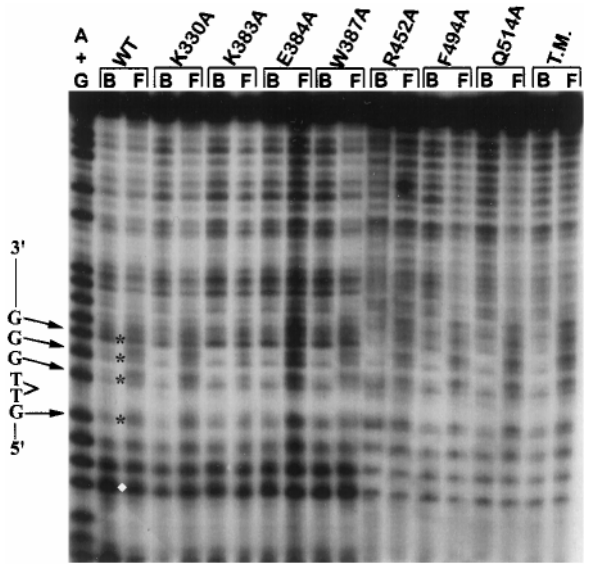


FIG. 4. **Ethylnitrosourea (*ENU*) interference pattern for the wild-type and substituted photolyases.** Substrate containing a thymine dimer and $^{32}$P-labeled at the 5′ end of the dimer-containing strand was treated with ethylnitrosourea, incubated with photolyase, separated into free and bound fractions by EMSA, cleaved at modified phosphates, and analyzed on a 12% denaturing polyacrylamide gel. A representative autoradiogram is shown. *A* + *G* denotes an A + G sequencing ladder. Photolyases are indicated by the mutant name wild type (*WT*) or K330A/E384AF/F494A (*T.M.*). For each photolyase, *B* is the bound fraction from an EMSA reaction, and *F* is the free (unbound) fraction. The 1st phosphate 5′ to the dimer and the 1st, 2nd, and 3rd phosphates 3′ to the dimer are indicated by ⋆ between the *WT* lanes. The band used to normalize the number of counts in each lane is indicated by the *white diamond*.

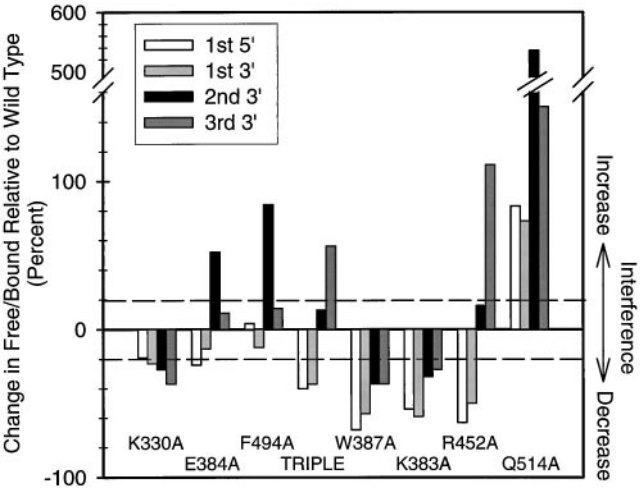


FIG. 5. **Quantitation of the ethylation interference data shown in Fig. 4.** For each band analyzed, the fraction ($free_{cpm}/bound_{cpm}$) for the wild-type enzyme was subtracted from the same fraction for the mutant enzyme, and the result was multiplied by 100. The legend within the figure refers to positions of the phosphates relative to the pyrimidine dimer. The *dashed lines above* and *below* the *x* axis indicate 20% change, which is the minimum considered to be significant and reproducible.

all sites, suggesting that interactions between the enzymes and phosphates in the dimer-containing strand have changed along the entire binding interface. Despite this general similarity, the two photolyases displayed distinctive differences in the interference pattern at specific phosphates indicating that the protein-DNA interface is uniquely altered in each mutant. Furthermore the relative magnitude of these effects is consistent with the relative decrease in $K_A$. Mutants E384A, F494A, and the triple mutant (K330A/E384A/F494A) displayed increased interference at the second or third phosphate 3′ to the dimer and, in the cases of E384A and the triple mutant, decreased interference at one or both phosphates flanking the dimer. Thus it appears that, in this second class of mutant, loss of interactions within the active site cavity attenuates photolyase-DNA phosphate interactions at sites adjacent to the dimer and enhances dependence on interactions at the 2nd and 3rd phosphates 3′ to the dimer. Overall the changes in ethylation interference patterns seen with these mutants indicate that residues within the active site cavity play a role in orienting the dimer-containing strand along the entire length of the binding interface.

Ethylation interference patterns similar to those obtained for the active site cavity mutants were also observed when residues outside of the cavity were altered (Fig. 5). K383A exhibited a general decrease in interference at all sites, similar both qualitatively and quantitatively to the pattern seen with the W387A mutant. In the modeled structure the side chain of $Lys^{383}$ packs against the edge of the $Trp^{387}$ indole ring, and therefore changing one of these residues to Ala may affect the position of the other. The ethylation interference pattern of the R452A mutant resembled that of the triple mutant (K330A/E384A/F494A) suggesting that, despite its surface location, $Arg^{452}$ plays a key role in orienting the dimer in the active site cavity. This interpretation is supported by the results of quantum yield experiments discussed below. The Q514A mutant displayed an unusual pattern in that interference increased at all sites. The simplest explanation is that one or more strong nonphosphate contacts have been lost in the mutant and that, as a result, interactions with phosphates contribute relatively more to the overall binding energy.

*The Effects of Substitution Mutations on Quantum Yield*—Substitutions that affect the electronic environment within the active site, the positioning of the dimer within the active site, or the equilibrium between the flipped and nonflipped state potentially alter the efficiency of photolysis. Therefore we determined the quantum yield for photolysis by each substituted enzyme and compared it to the quantum yield of the wild-type enzyme. Each of the purified proteins was bound to dimer-containing substrate, and the complex was photoreactivated with 365 nm light in increments of 25 J/m$^2$. The amount of DNA repaired by photolyase was quantified by electrophoretic mobility shift assay. Under the experimental conditions employed, ≥70% of the substrate was bound prior to exposure to limiting photoreactivating light. Thus multiple cycles of binding and photoreactivation by a single enzyme molecule do not contribute significantly to the results obtained.

The quantum yield value obtained for each photolyase relative to wild-type is shown in Table II. Among the substitutions within the cavity, K330A and F494A had little or no effect on the quantum yield. In contrast, E384A, the triple substitution mutant, and W387A displayed 60–80% reductions in quantum yield relative to the wild-type enzyme. The $Glu^{384}$ side chain lies in the floor of the active site cavity (Fig. 6), and its negative charge may assist in directing electron transfer from $FADH^-$ to the dimer and away from solvent. The further reduction in quantum yield seen with the triple substitution mutant may reflect both loss of this effect and, consistent with the DNA binding defect, reorientation of the dimer in the active site. $Trp^{387}$ is predicted to make van der Waals contact with the dimer (Ref. 14 and Fig. 6); its loss may permit reorientation of the dimer in the binding pocket or alter the equilibrium between the flipped and nonflipped state. The most surprising result of the quantum yield study was the 60% decrease in quantum yield seen with the R452A mutant. $Arg^{452}$ lies outside

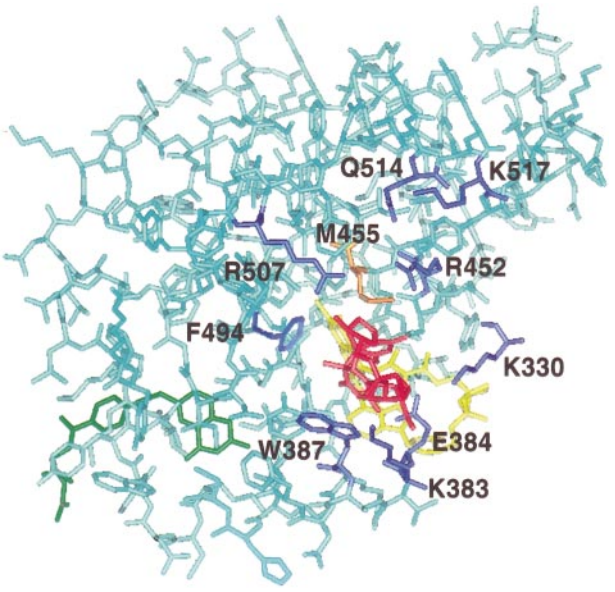


FIG. 6. **The modeled active site and DNA binding surface of *S. cerevisiae* photolyase with a pyrimidine dimer docked in the active site cavity.** Amino acids examined by mutagenesis in this and a previous study (9) are shown in *blue*. Met$^{455}$, which is also predicted to interact with the dimer but has not been mutated, is shown in *orange*; $FADH^-$ is shown in *yellow*; the folate chromophore is shown in *green*, and the dimer is shown in *red*. To show more clearly the relationship of the dimer bases to residues in the cavity, the structure has been rotated approximately −25° around the *y* axis relative to the view shown in Fig. 3. The entire modeled region is shown.

of the active site cavity, and thus alanine substitution was not expected to affect the electronic environment within the active site. Indeed, none of the other substitutions outside of the cavity significantly changed the quantum yield (Table II). An attractive explanation is that interaction between Arg$^{452}$ and DNA residues flanking the dimer plays a crucial role in establishing or stabilizing the dimer in the flipped state.

## DISCUSSION

*A Model for Dimer Binding by Photolyase*—Approximately 50% of the total energy of enzyme-substrate complex formation between photolyase and dimer-containing DNA comes from interaction between the enzyme and elements of the dimer (7, 12, 13). If, as proposed by Park *et al.* (14), the dimer resides within the cavity leading from the flavin chromophore to the surface of the enzyme, interactions with residues lining the cavity should contribute significantly to the binding energy. The results reported here provide direct experimental confirmation of this prediction. Alanine substitution at each of four sites (Lys$^{330}$, Glu$^{384}$, Phe$^{494}$, and Trp$^{387}$) within the active site cavity reduces substrate binding. Because these residues lie too deeply buried in the pocket to interact with normal B-DNA, the only explanation for these results is that either the enzyme or the substrate undergoes a dramatic structural alteration that places these amino acids within interacting distance with DNA. A large scale conformational change in the enzyme is highly unlikely. With the exception of Lys$^{330}$, all of the cavity residues probed here lie within helices that are held firmly in place by multiple interactions with neighboring structural elements, and movement of these helices toward the surface would disrupt multiple interactions with the flavin chromophore. These considerations, combined with the structural and chemical complementarity of the active site to the dimer, provide strong evidence that the cavity in photolyase identified by Park *et al.* (14) is indeed the binding site for an extrahelical pyrimidine dimer.

A model of a pyrimidine dimer docked in the active site cavity of the yeast Phr1 photolyase is shown in Fig. 6. This model is based upon the crystal structure of a thymine dimer (23) and the modeled yeast photolyase structure; until the structure of a pyrimidine dimer in double-stranded DNA is solved at atomic resolution, this model provides a useful context for interpreting the results of this and previous structure-function studies (9, 24). The 5′ → 3′ placement of the dimer is predicated upon our observation that the enzyme interacts more extensively with DNA residues 3′ to the dimer and upon the locations of mutations that reduce DNA binding (this work and Refs. 9, 12, and 13). In this model the 5′ base in the dimer is involved in $\pi$-$\pi$ stacking interactions with Trp$^{387}$; the methyl group of the 5′ base is sandwiched into a hydrophobic pocket between Trp$^{387}$ and Phe$^{494}$; the methyl group of the 3′ base is involved in hydrophobic interactions with Phe$^{494}$; N-3 of both bases are within hydrogen bonding distance of O-$\epsilon$ of Glu$^{384}$, and the phosphate 5′ to the dimer is within hydrogen bonding distance of the side chains of Lys$^{330}$ and Lys$^{383}$. Other potential interactions involving the dimer include a hydrogen bond between the exocyclic amine of the adenine base in FAD and O-4′ of the 5′ dimer, and a "hydrogen bond" (25) between the sulfur in Met$^{455}$ and the methyl group of the 3′ base. Arg$^{452}$, Gln$^{514}$, Arg$^{507}$, and Lys$^{517}$ lie on the surface of the enzyme immediately outside of the active site cavity and are positioned to interact with DNA residues 3′ to the dimer. Alanine substitution at each of these sites reduces the affinity of the enzyme for dimer-containing DNA (this work and Ref. 9). This model, in conjunction with the data reported here and in our previous work (9), provides insight into the mechanisms used by the enzyme to discriminate between different types of bases in dimers and between nondamaged and damaged DNA.

*Substrate Recognition and Discrimination*—A number of interactions within the active site cavity are predicted to contribute to base discrimination. Phe$^{494}$ interacts with methyl groups on both thymidines in the dimer, and loss of these interactions should decrease binding. Consistent with this prediction, the affinity of *E. coli* photolyase for dUU dimers in DNA is approximately 3-fold lower than for TT dimers (7), and as we have shown here, alanine substitution of Phe$^{494}$ results in a similar decrease in binding. An 8-fold decrease in binding affinity (compared with TT dimers) has been reported for C-containing dimers (7). According to the model, this likely reflects not only loss of interactions with Phe$^{494}$ but also loss of hydrogen bonds between FAD and O-4′ of the 5′ thymine in the dimer and between Glu$^{384}$ and the protonated N-3 of both thymines. In addition steric clash between the exocyclic amine group of C and the exocyclic amine of adenine in FAD is likely to constrain the approach of C-containing dimers to FAD. This may contribute to the 20-fold lower quantum yield for photolysis of CC dimers relative to TT dimers (7). Overall the structure of the active site cavity favors binding of TT dimers, which are the predominant cyclobutane-type dimers formed following UV (26).

Interactions with residues within the active site cavity also contribute to discrimination between dimer and nondimer DNA. Trp$^{387}$ is the single most important "discrimination" residue identified here and likely contributes to substrate discrimination in two ways. (i) Because the two bases in the dimer are covalently linked by the rigid cyclobutane ring, parallel alignment of the 5′ base and Trp$^{387}$ side chain simultaneously orients both bases thereby establishing the full repertoire of interactions within the active site cavity. (ii) Stacking interactions between Trp$^{387}$ and the 5′ base lower the energetic cost of dimer flipping by partially compensating for base stacking interactions that are disrupted when the dimer is moved out of

TABLE III
*Conservation of selected residues in photolyases*

| Location and residue number in *S. cerevisiae* Phr1 photolyase | Residue found at equivalent position in class of photolyase | | |
|---|---|---|---|
| | Class I[a] | Class II[a] | 6–4[b] |
| Inside active site cavity | | | |
| 330 | Arg, Lys, His | Arg | Lys, Asn |
| 384 | Glu, Gln | Glu | Gln |
| 387 | Trp | Arg, Asn | Trp |
| 455 | Met | Met | His |
| 494 | Trp, Phe | Pro | Trp |
| Outside active site cavity | | | |
| 383 | Gly, Gln, Arg, Asn, Lys, Ser | Arg, Glu | Leu, Ile |
| 452 | Arg | Phe, Tyr | Leu |
| 507 | Arg | Ser, Cys, Glu | Arg |
| 514 | Gln | Gln, Met, Arg | Phe |
| 517 | Arg, Lys | Ala, Lys | Lys |

[a] Based upon the alignment of the class I and class II photolyases in Ref. 34.
[b] Based upon alignment of the predicted amino acid sequences of the 6–4 photolyases from *A. thaliana* (38) and *D. melanogaster* (39) using the alignment program CLUSTAL W.

the helix. It should be noted that most of the interactions in the active site cavity can also occur when two nondimerized pyrimidines are flipped into the helix. This suggests that much of the binding specificity conferred by interactions within the active site cavity arises from differences in the energy cost of flipping two unlinked bases *versus* a dimer. Several studies suggest that the presence of a dimer in a DNA helix weakens stacking interactions with adjacent bases and hydrogen bonding with the partners of the dimerized bases (27–29), and thus the energetic cost of flipping a dimer out of the helix and into the active site cavity should be lower than the cost of flipping two noncovalently linked pyrimidines. The free energy contributed by interactions between cavity residues and the dimer is sufficient to stabilize the dimer in the flipped state but is not sufficient to stabilize two noncovalently linked pyrimidine bases flipped out of the helix. This line of reasoning suggests that for the W387A mutant and the triple mutant (K330A/E384A/F494A) the equilibrium between the flipped and nonflipped dimer is shifted. Presumably flipping of the dimer is accompanied by repositioning of phosphates immediately surrounding the dimer, as has been seen for other flipped nucleotides (30, 31). Both the triple mutant and the W387A mutant display large decreases in ethylation interference at these sites, consistent with loss of the phosphate positioning that is unique to the flipped state. We emphasize that decreased ethylation interference in these mutants is a secondary effect of loss of contacts within the active site cavity. The decrease in quantum yield seen with these mutants may likewise reflect a decrease in the equilibrium between the flipped and nonflipped state.

$Lys^{383}$, $Arg^{452}$, and $Gln^{514}$ lie outside of the active site cavity, and substitutions at each of these sites reduces both overall binding affinity as well as the ability of photolyase to discriminate between dimer-containing and nondamaged DNA. According to the model these residues contact regions immediately 5′ to the dimer ($Lys^{383}$) or 3′ to the dimer ($Arg^{452}$ and $Gln^{514}$). Both molecular modeling studies and NMR experiments suggest that in dimer-containing DNA the helix is distorted at the nucleotide 5′ to the dimer and the first and second nucleotides 3′ to the dimer (27, 28, 32). Thus there is an excellent correlation between the DNA sites that promote dimer-specific recognition and the location of photolyase residues that contribute to specific binding. As might be expected for loss-of-contact mutants at these sites, alanine substitution at $Lys^{383}$ or $Gln^{514}$ decreases both specific and nonspecific binding with the larger effect being seen on specific binding. In contrast, alanine substitution at $Arg^{452}$ increases nonspecific binding as well as decreases specific binding. This could reflect introduction of a new interaction that interferes with binding or, more likely in our opinion, loss of the $Arg^{452}$ side chain which interferes with binding to nondimer DNA. It is interesting to note that this mutant also exhibits a profound defect in the quantum yield for repair and a substantial and specific decrease in ethylation interference at phosphates immediately surrounding the dimer. These are characteristics shared with the $Trp^{387}$ mutant and the triple mutant (K330A/E384A/F494A) and suggest that, like these mutants, $Arg^{452}$ may play an important role in maintaining the dimer in the flipped orientation. We note that several DNA-binding proteins that "flip" nucleotides out of the helix do so by inserting one or more side chains into the helix, thereby displacing the base (31, 33). Whether this is the role of $Arg^{452}$ must await the cocrystal structure.

*Evolutionary Implications*—Two classes of CPD photolyases have been identified based upon sequence homology (34). Most microbial photolyases, including the *E. coli*, *A. nidulans*, and *S. cerevisiae* enzymes, are members of class I and share 25–43% sequence homology, whereas most photolyases from higher eukaryotes are members of class II and share 38–72% homology. Because the homology between enzymes in different classes is only 10–17%, it is pertinent to ask whether enzymes in these two classes employ common mechanisms to recognize and repair pyrimidine dimers. While direct information on the three-dimensional structure of class II enzymes is lacking, several lines of evidence support a common mechanism. All of the enzymes require reduced FAD to carry out photolysis (4, 34). The *M. thermoautotrophicum* photolyase, the only representative of class II enzymes that has been characterized extensively with respect to DNA binding, contacts the same phosphates surrounding the dimer as do the yeast and *E. coli* enzymes (35). Finally, despite the low level of overall homology between the two classes of enzymes, there is striking conservation of amino acids lining the active site cavity, and to a lesser extent of amino acids that interact with flanking DNA residues (Table III). Even more surprising is the sequence conservation between residues in the active site cavity of the class I photolyases and the (6-4) photolyases (Table III). Evidence has been presented suggesting that the (6-4) photolyases also flip their substrates out of the DNA helix (36). However, the structure of the binding site must be sufficiently different to exclude pyrimidine dimers that are not efficiently bound by (6-4) photolyases (2, 37). Nevertheless, of the five residues within the cavity that are predicted to contact the dimer in CPD photolyases, four are conserved in the (6-4) photolyases. This is consistent with the proposed evolution of the class I CPD and (6-4) photolyases from a common ancestral gene (38, 39) and further suggests that the different binding specificities of the enzymes entail surprisingly few changes in the active site cavity. The cocrystal structures of these two types of photolyases should

provide insight into the crucial interactions required for such discrimination.

*Acknowledgments*—We thank Dr. Hengming Ke for assistance with the protein modeling; Dr. Hee-Won Park for providing the structure of the pyrimidine dimer; Drs. Aziz Sancar and Xiaodong Zhao for dimer substrate and useful discussions; and Kalpana Kasala for technical assistance.

REFERENCES

1. Sancar, A. (1996) in *Annual Review of Biochemistry* (Richardson, C. C., Abelson, J. N., and Raetz, C. R. H., eds) pp. 43–81, Annual Reviews, Inc., Palo Alto, CA
2. Todo, T., Takemori, H., Ryo, H., Ihara, M., Matsunaga, T., Nikaido, O., Sato, K., and Nomura, T. (1993) *Nature* **361,** 371–374
3. Brash, D. E., Franklin, W. A., Sancar, G. B., Sancar, A., and Haseltine, W. A. (1985) *J. Biol. Chem.* **260,** 11438–11441
4. Sancar, A. (1994) *Biochemistry* **33,** 2–9
5. Sancar, G. B., Jorns, M. S., Payne, G., Fluke, D. J., Rupert, C. S., and Sancar, A. (1987) *J. Biol. Chem.* **262,** 492–498
6. Sancar, G. B. (1990) *Mutat. Res.* **236,** 147–160
7. Kim, S.-T., and Sancar, A. (1991) *Biochemistry* **30,** 8623–8630
8. Husain, I., and Sancar, A. (1987) *Nucleic Acids Res.* **15,** 1109–1120
9. Baer, M. E., and Sancar, G. B. (1993) *J. Biol. Chem.* **268,** 16717–16724
10. Li, Y. F., and Sancar, A. (1990) *Biochemistry* **29,** 5698–5706
11. Kim, S.-T., Malhotra, K., Smith, C. A., Taylor, J.-S., and Sancar, A. (1993) *Biochemistry* **32,** 7065–7068
12. Baer, M., and Sancar, G. B. (1989) *Mol. Cell. Biol.* **9,** 4777–4788
13. Husain, I., Sancar, G. B., Holbrook, S. R., and Sancar, A. (1987) *J. Biol. Chem.* **262,** 13188–13197
14. Park, H.-W., Kim, S.-T., Sancar, A., and Deisenhofer, J. (1995) *Science* **268,** 1866–1872
15. Sancar, G. B. (1985) *Nucleic Acids Res.* **13,** 8231–8246
16. Sancar, G. B., Smith, F. W., and Heelis, P. F. (1987) *J. Biol. Chem.* **262,** 15457–15465
17. Taylor, J.-S., Brockie, I. R., and O'Day, C. L. (1987) *J. Am. Chem. Soc.* **109,** 6735–6742
18. Segel, I. H. (1975) *Enzyme Kinetics*, pp. 100–120, John Wiley & Sons, Inc., New York
19. Siebenlist, U., Simpson, R. B., and Gilbert, W. (1980) *Cell* **20,** 269–281
20. Maxam, A. M., and Gilbert, W. (1980) *Methods Enzymol.* **65,** 499–560
21. Tamada, T., Kitadokoro, K., Higuchi, Y., Inaka, K., Yasui, A., de Ruiter, P. E., Eker, A. P. M., and Miki, K. (1997) *Nat. Struct. Biol.* **4,** 887–891
22. Payne, G., Wills, M., Walsh, C. T., and Sancar, A. (1990) *Biochemistry* **29,** 5706–5711
23. Cadet, J., Voituriez, L., Hruska, F. E., and Grand, A. (1985) *Biopolymers* **24,** 897–903
24. Kim, S.-T., Li, Y. F., and Sancar, A. (1992) *Proc. Natl. Acad. Sci. U. S. A.* **89,** 900–904
25. O'Gara, M., Klimasauskas, S., Roberts, R. J., and Cheng, X. (1996) *J. Mol. Biol.* **261,** 634–645
26. Patrick, M. H., and Rahn, R. O. (1976) in *Photochemistry and Photobiology of Nucleic Acids* (Wang, S. Y., ed) pp. 35–95, Academic Press, New York
27. Pearlman, D. A., Holbrook, S. R., Pirkle, D. H., and Kim, S. H. (1985) *Science* **227,** 1304–1308
28. Broyde, S., Stellman, S., and Hingerty, B. (1980) *Biopolymers* **19,** 1695–1701
29. Hayes, F. N., Williams, D. L., Ratliff, R. L., Varghese, A. J., and Rupert, C. S. (1971) *J. Am. Chem. Soc.* **93,** 4940–4943
30. Vassylyev, D. G., Kashiwagi, T., Mikami, Y., Ariyoshi, M., Iwai, S., Ohtsuka, E., and Morikawa, K. (1995) *Cell* **83,** 773–782
31. Slupphaug, G., Mol, C. D., Kavli, B., Arvai, A. S., Krokan, H. E., and Trainer, J. A. (1996) *Nature* **384,** 87–92
32. Taylor, J. S., Garrett, D. S., Brockie, I. R., Svoboda, D. L., and Telser, J. (1990) *Biochemistry* **29,** 8858–8866
33. Reinisch, K. M., Chen, L., Verdine, G. L., and Lipscomb, W. N. (1995) *Cell* **82,** 143–153
34. Yasui, A., Eker, A. P. M., Yasuhira, S., Yajima, H., Kobayashi, T., Takao, M., and Oikawa, A. (1994) *EMBO J.* **13,** 6143–6151
35. Kiener, A., Husain, I., Sancar, A., and Walsh, C. T. (1989) *J. Biol. Chem.* **264,** 13880–13887
36. Zhao, X., Liu, J., Hsu, D. S., Zhao, S., Taylor, J.-S., and Sancar, A. (1997) *J. Biol. Chem.* **272,** 32580–32590
37. Uchida, N., Mitani, H., Todo, T., Ikenaga, M., and Shima, A. (1997) *Photochem. Photobiol.* **65,** 964–968
38. Nakajima, S., Sugiyama, M., Iwai, S., Hitomi, K., Otoshi, E., Kim, S.-T., Jiang, C.-Z., Todo, T., Britt, A. B., and Yamamoto, K. (1998) *Nucleic Acids Res.* **26,** 638–644
39. Todo, T., Ryo, H., Yamamoto, K., Toh, H., Inui, T., Ayaki, H., Nomura, T., and Ikenaga, M. (1996) *Science* **272,** 109–112